Nanoparticulated WO3/NiWO4 Using Microcrystalline Cellulose as a Template and Its Application As Auxiliary Co-catalyst to Pt for Ethanol and Glycerol Electro-Oxidation to Produce Green Hydrogen

Munique G. Guimarães , Julio L. Macedo , José J. Linhares , Grace F. Ghesti *

Posted Date: 27 November 2023

doi: 10.20944/preprints202311.1641.v1

Keywords: nanocrystalline cellulose; microcrystalline cellulose; nickel oxide; zirconia; electrocatalysis; ethanol; glycerol

Article

Nanoparticulated $WO_3/NiWO_4$ Using Microcrystalline Cellulose as a Template and Its Application as Auxiliary Co-Catalyst to Pt for Ethanol and Glycerol Electro-Oxidation to Produce Green Hydrogen

Munique G. Guimarães [1], Julio L. Macedo [1], José J. Linares [2] and Grace F. Ghesti [2,*]

[1] Laboratory of Bioprocesses Brewing Technology and Catalysis in Renewable Energy, Institute of Chemistry, University of Brasilia, Brasília-DF, 70910-900, Brazil

[2] Laboratory of Chemical Processes Development, Institute of Chemistry, University of Brasilia, Brasilia, DF, 70910-900, Brazil

* Correspondence: grace@unb.br

Abstract: This manuscript presents the result of utilizing cellulose as a template to prepare nanosized WO_3-$NiWO_4$ and its application as co-catalysts in Pt/WO_3-C and Pt/WO_3-$NiWO_4$-C for ethanol and glycerol electro-oxidation. Microcrystalline cellulose was hydrolyzed with phosphotungstic acid ($H_3PW_{12}O_{40}$) to prepare the nanosized template of crystalline cellulose. Next, the template was impregnated with $Ni(NO_3)_2$, rendering a precursor material that is subsequently air-calcinated, removing the carbon-template material to obtain the nanometric WO_3 and $NiWO_4$. Elemental analysis confirmed the coexistence of nickel and tungsten, whereas the thermal analysis evidenced the high thermal stability of these materials. The X-ray diffractograms displayed crystal facets of WO_3 and, when added Ni, of $NiWO_4$. The transmission electron micrographs corroborated the formation of nanosized particles with average particle sizes close to 50 nm. Finally, to apply this material, Pt/WO_3-C and Pt/WO_3-$NiWO_4$-C were prepared and used in ethanol and glycerol electro-oxidation in alkaline medium, observing a promotional effect of the oxide and tungstate by reducing the onset potential and increasing the current density. These materials show great potential to produce clean electricity or green hydrogen contributing to energetic transition.

Keywords: nanocrystalline cellulose; microcrystalline cellulose; nickel oxide; zirconia; electrocatalysis; ethanol; glycerol

1. Introduction

Biomass is gaining more relevance in the worldwide energy panorama [1]. In the transition towards a sustainable energy reality in the coming years, biomass is expected to account for up to 66% of the renewable energy offer. Nevertheless, biomass processing produces wastes whose treatment and possible valorization are mandatory to make its entire cycle of use sustainable [2]. As a reference figure, for every ton of sugarcane processed, 280 kg of bagasse are obtained [3,4], primarily used to produce the energy required in the sugar/ethanol factory [5]. However, other alternatives are possible, such as producing second-generation ethanol from biomass wastes [6,7] or fabricating nanocellulose (NC) from acid hydrolysis of the cellulose fibers [8]. Phosphotungstic acid (PWA) is a promising acid catalyst due to its low toxicity, easy recycling, high Bronsted acidity, and thermal stability [9].

NC has many applications in medicine, film preparation, sensors, water purification, packaging, polymer composites, energy storage, catalysis, and environmental remediation [10,11]. One particular application of NC is its use as a template for preparing metallic compounds, for instance, metal oxides, with controlled size, structure, and/or porosity, as recently reviewed by Anžlovar and Žagar [12]. As stated by the authors, some oxides are TiO_2 (the most extendedly prepared), ZnO,

Fe_2O_3, CuO, Mn_3O_4, Nb_2O_5, Co_3O_4, SnO_2 and mixed oxides such as $Cu_{0.5}Co_{0.5}Fe_2O_4$, or $BaFe_{12}O_{19}/CoFe_2O_4$. The process consists of mixing the metal oxide precursor with the NC and, in sequence, applying a thermal treatment in an air atmosphere to obtain the oxide material, or even if the NC is pyrolyzed, we can get a metallic (oxide) material supported on carbon. Metal oxides have vast applications, including catalysis, gas sensing, microelectronics, environmental remediation, energy storage, ceramic fabrication, medicine, and sensors [13]. Energy and environmental applications are becoming more relevant due to the urgent necessity of changing our current energy mix from mostly fossil to renewable energy sources [14].

In this sense, fuel cells and electrolyzers are receiving more attention due to the possibility of producing energy or green hydrogen, respectively, from renewable sources. Hydrogen is the most widely used fuel in fuel cells. Nevertheless, it faces some shortcomings, such as its production, nowadays mostly from fossil fuels [15], as well as safety and storage [16]. In the case of the electrolysis, the main limitation comes from the final high price of the produced hydrogen from water electrolysis due to the requirement of high cell voltages [17], in addition to the hydrogen limitations. In this sense, replacing the oxidant, hydrogen in fuel cells, or water in electrolyzers, with liquid alcohols could solve the storage, transportation, and, partially, safety issues. These replacements give rise to the Direct Alcohol Fuel Cells, and the Alcohol Electroreformers, producing electricity and hydrogen from the liquid alcohol electro-oxidation. In particular, ethanol and glycerol are of interest as they are made from biomass-based processes, sugarcane fermentation in the first case [18], and a by-product of biodiesel synthesis for the latest [19].

Ethanol and glycerol electro-oxidation undergo sluggish kinetics due to the complexity of their oxidation mechanisms, involving several steps: alcohol adsorption, dehydrogenation, formation of strongly adsorbed alcoholic species on the surface of the catalyst, addition of oxygenated species from neighboring actives sites, and C-C cleavage [20]. At the low temperatures used in the Polymer Electrolyte Membrane Fuel Cells/Electroreformers, platinum or platinum-based electrocatalysts are recognized as the reference material, given their high catalytic performance [21–23]. Nonetheless, platinum is expensive and scarce, as well as it undergoes severe deactivation from the adsorbed residues produced during the alcohol electro-oxidation.

One approach to overcome this shortcoming is the addition of a co-catalyst to Pt, such as the metal oxides, which can exert a double promotional effect on Pt: a) electronic effect, in which the electron interaction between the metal oxides and Pt alters the Pt electronic structure, reducing the adsorption strength of the adsorbates formed during the alcohol oxidation [24], and b) bifunctional mechanism, where the oxyphilic metal oxides can donate oxygenated groups to the neighboring Pt sites to promote the oxidation and release of the adsorbed species at lower potential than Pt, refreshing the Pt surface [25]. One metal oxide with an intense promotional effect on Pt for alcohol electro-oxidation, both in acid and alkaline medium, is nickel oxide [26]. Furthermore, we can add an extra promotional effect by using oxides with a prominent spillover effect, such as WO_3 [27–31], in which WO_3 can uptake the Pt-H_{ads} formed in the initial stages of the ethanol and glycerol electro-oxidation, in addition to the supply of OH_{ads} species. Moreover, if nickel and tungsten precursors are calcinated together, the binary metal oxide NiO/WO_3, nickel tungstate ($NiWO_4$) can be formed, a material with high stability, low corrosion, and electrocatalytic activity [32,33]. Indeed, $NiWO_4$ has been applied as catalyst for hydrogen and oxygen evolution reactions [34–36], as well as hydrogen oxidation and oxygen reduction in acidic medium [37], and alkaline medium [38], acting as co-catalyst with Pt. To the authors' knowledge, there is a sole application to the methanol electro-oxidation in acid medium, proposed by Adzic and Marinkovic [39] in 2001, with no further exploration of its potential for alcohol oxidation. Furthermore, the presence of segregated NiO cannot be disregarded. This oxide promotes the Pt activity for ethanol and glycerol electro-oxidation [26].

With these antecedents, this study aims to prepare multifunctional trimetallic catalysts based on synthesizing nanometric binary metal oxides, WO_3 (**labeled hitherto TO**) and $NiWO_4$ (**labeled hitherto NiT**), using nanocrystalline cellulose (NCC) as a template. For this purpose, in the first step, NCC is prepared from the acid hydrolysis of microcrystalline cellulose (MCC) in phosphotungstic acid (PWA, $H_3PW_{12}O_{40}$), rendering a mixed material formed by PWA/NCC. This composite material

Preprints (www.preprints.org) | NOT PEER-REVIEWED | Posted: 27 November 2023 doi:10.20944/preprints202311.1641.v1

was used as a template for preparing binary oxide. The PWA/NCC was impregnated with the nickel precursor and calcinated to obtain the binary oxide NiT. The prepared materials were physicochemically characterized by CNH analysis, Energy Dispersive Spectroscopy (EDS) to verify the metal loading and proportions of each metal, X-Ray Diffractometry (XRD) to see the crystallinity of the samples, and Transmission Electron Microscopy (MET) to visualize the micro/nanostructure of the prepared materials. Afterward, Pt nanoparticles were deposited onto a mixture of NiT and the carbon support to improve the electrical conductivity (Vulcan XC-72R). Also, Pt nanoparticles were deposited in a mixture of TO and the carbon support and, as a reference, directly onto the carbon support. The prepared materials were tested for ethanol and glycerol electro-oxidation in alkaline medium to evaluate their performance and potential applications for these relevant electrochemical reactions.

2. Results

2.1. Nanocrystalline cellulose

Table S1 (Supplementary Material) summarizes the main immediate analysis of the raw matter used in this study, MCC. The most relevant result is the absence of ash material. This is important if we consider that the subsequent NCC used as a template is not expected to leave any residue in the prepared electrocatalyst. Figure 1 collects the corresponding results of the final composition of the NCC after the acid hydrolysis with PWA.

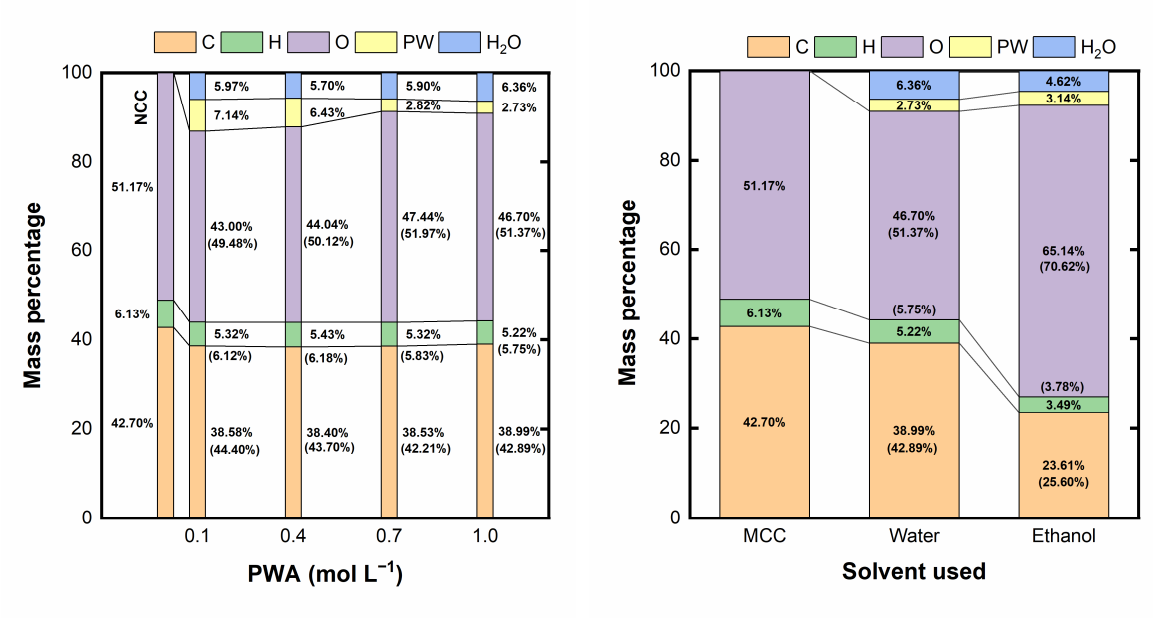

Figure 1. Mass percentage of the different elements as a function of (a) concentration of PWA in water, and (b) solvent used in the hydrolysis for 1 mol L^{-1} of PWA (PW is the fraction of phosphorous and tungsten from the PWA; values in parenthesis represents the relative percentages of C, H, and O to compare with the original MCC).

As observed in Figure 1(a) referred to the aqueous hydrolysis, the treatment with PWA inserts phosphorous and tungsten in the NCC due to the acid used in the hydrolysis. In parallel, the amount of PW that remained in the NCC structure reduces as the PWA hydrolysis concentration increases, without significant variations in the C, H, and O relative percentages compared to the original MCC. On the other hand, the results displayed in Figure 1(b) show a relevant change in the percentages of C and O when ethanol is used as solvent using a PWA concentration of 1 mol L^{-1}, with a significant

Preprints (www.preprints.org) | NOT PEER-REVIEWED | Posted: 27 November 2023 doi:10.20944/preprints202311.1641.v1

drop in the C percentage accompanied by an increase in the O percentage. Moreover, there is an increase in the PW percentage, augmenting from 2.73 to 3.14% when water is replaced by ethanol.

The thermal stability of the CNC and the original MCC is compared in Figure S1. MCC and NCC present similar shapes with a slight decrease in the onset temperature of the polysaccharide degradation. Figure S2 shows the diffractograms of the MCC and NCC. The diffraction patterns match each other, indicative of the preservation of the crystalline structure after the PWA hydrolysis. Figure S3 displays the MCC and NCC's MET images after hydrolysis. The MCC processing by acid hydrolysis results in a significant reduction of the particle size. From the combination of all the results, in terms of smaller particles, maintaininsimg the crystalline structure in a nanometric range, and its thermal stability, the NCC prepared with PWA 1 mol L^{-1} in water was elected as the best template material for depositing the nickel particles.

2.2. Nanosized NiT/TO

The sequence for preparing the binary metal oxides involved the calcination of the $Ni(NO_3)_2$-impregnated NCC for two different impregnation times (1 and 6 h) and two impregnation solvents (ethanol and water; more details in section 4). After the corresponding calcination for 8 h at 600 °C, temperature estimated from the thermal analysis of the Ni-impregnated samples to guarantee the NCC template decomposition, Figure 2 shows the metal weight percentages of Ni and W remaining in the calcinated samples (no phosphorous detected, probably dissolved during the washing process). This figure gives an idea of the efficiency of the nickel anchorage onto the NCC template.

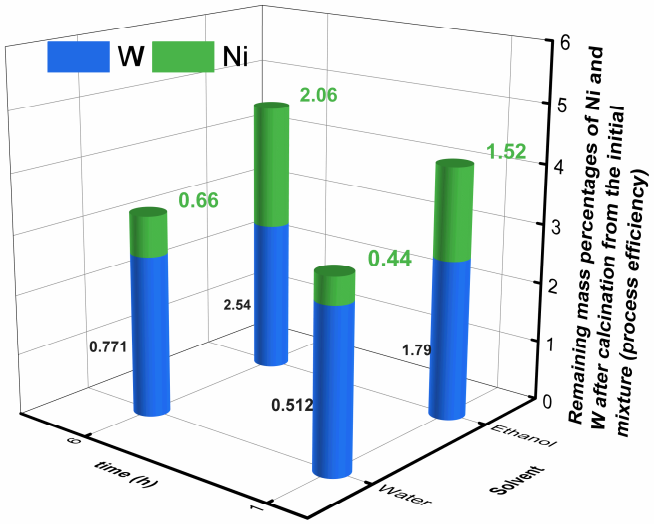

Figure 2. Ni and W remaining after the deposition and calcination process. Numbers in the upper part of the bars represent the percentage of Ni deposited from the initial sample. In contrast, the numbers in the center of the blue bar represent the Ni/W atomic ratio.

As observed, the highest amount of nickel is obtained when ethanol is used as solvent to anchor the Ni onto the NCC template. Also, it is interesting to look at the values of the Ni/W ratio, given that we aim at preparing a binary metal oxide. Water use favors a higher proportion of W, contrarily to ethanol, in which the anchorage of Ni is favored. Given that we aim to prepare a binary metal oxide with the highest Ni content and an equilibrated Ni/W atomic ratio, using ethanol and the impregnation for 1 h seems to be the most suitable condition.

Figure 3 displays the XRD diffraction patterns of the prepared mixed oxides after calcination (nomenclature: solvent: E: ethanol, W: water; the numbers indicate the impregnation time). The vertical lines represent the NiO, TO, and NiT diffraction peaks. As can be observed, all the materials are formed by a combination of TO and NiT, with no segregated NiO phases. The proportion and

Preprints (www.preprints.org) | NOT PEER-REVIEWED | Posted: 27 November 2023 doi:10.20944/preprints202311.1641.v1

intensity of each phase depend on the amount of each metal present in the final calcinated product. Also, the solvent and time used to anchor the Ni precursor onto the NCC impact in the detected phases. In the E1 sample, the most intense peak, at a 2θ angle of 31°, corresponds to the (111) facet of the monoclinic crystal structure of NiT [40,41], as in the E6 material. In the case of the W1 material, the most intense peak, at 28,3°, is attributed to the (200) facet of the hexagonal crystal structure of TO [42]. Finally, the W6 material presents the highest peak at 23.1 in a sequence of three consecutive intense peaks. Such a pattern fits well with the monoclinic TO [43]. In summary, all the samples display peaks attributable to TO in a combination of orthorhombic, monoclinic, and hexagonal TO, along with NiT (despite the mixture of TO and NiT, the samples are identified as NiT). Table 1 collects the corresponding average crystallite size after applying Scherrer's equation [44]. Finally, Figure S4 shows the TEM images of the prepared materials for the different impregnation conditions.

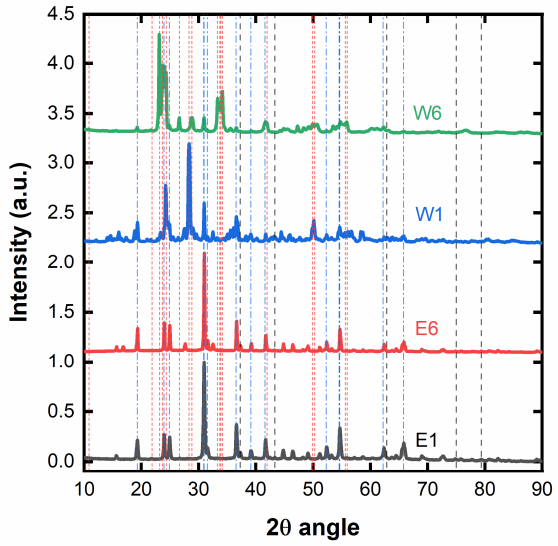

Figure 3. XRD pattern of the different mixed oxide samples as a function of the solvent used to prepare the mixed oxides and the times applied. Dash black lines represent the NiO diffraction peaks, red short dash lines represent the TO diffraction peaks, whereas blue dash and dot lines represent the NiT diffraction peaks.

Table 1. Average crystallite size of the different prepared oxide materials.

Sample	TO phase (nm)	NiT phase (nm)
E1	23.5	24.8
E6	43.8	45.3
W1	30.9	31.3
W6	41.1	38.6

The average crystallite size and the TEM confirm that the E1 condition leads to the smallest crystalline and particle sizes and the most homogeneous particle distribution.

2.3. Pt/TO-C and Pt/NiT-C electrocatalysts

Figure 4 displays the XRD pattern of the prepared Pt/TO-C and Pt/NiT-C electrocatalysts. As can be observed, the typical peaks attributed to the Pt fcc (111), (200), (200), (311), and (222) are present at 39.8, 46.2, 67.5, 81.3, and 85.7°, respectively. These peaks' presence confirms platinum's deposition on the combined support of carbon and the TO and NiT. The average crystallite sizes are 3.2 and 2.5 nm, estimated using Scherrer's equation.

Preprints (www.preprints.org) | NOT PEER-REVIEWED | Posted: 27 November 2023 doi:10.20944/preprints202311.1641.v1

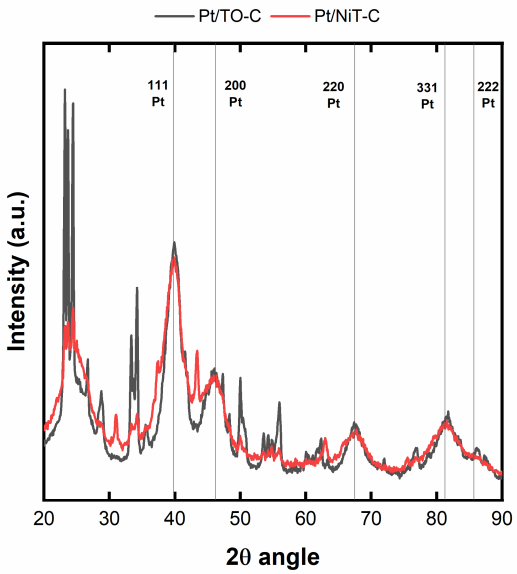

Figure 4. XRD pattern of the Pt-based electrocatalysts prepared on the TO-C and NiT-C supports (Lines represent the main Pt fcc diffraction peaks).

Figure 5 displays the blank voltammograms of the prepared materials compared to the reference Pt/C. The peaks associated with the hydrogen adsorption/desorption appear for all the materials, as well as the formation of the Pt oxide (including the formation of the Pt-OH_{ads} prelayer at approx. −0.15 V vs. MMO (Hg/HgO/KOH, mercury/mercury oxide reference electrode)), and their corresponding reduction peaks in the cathodic scan.

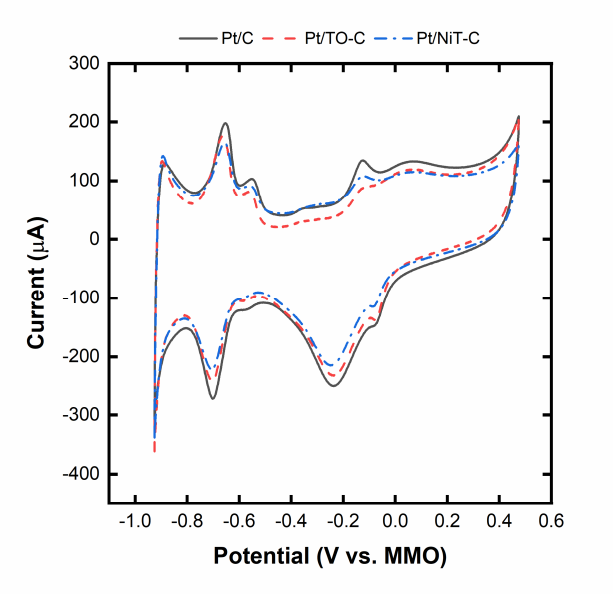

Figure 5. Blank voltammograms of the prepared electrocatalysts in 1 mol L^{-1} KOH.

Figure 6 displays the ethanol and glycerol electro-oxidation curves in acid and alkaline medium for the different materials. The addition of TO, and especially NiT-TO, significantly increases the ethanol and glycerol electro-oxidation activity. To have a better insight, Table 2 collects the value of the onset potential and the maximum current for each catalyst. As can be seen, there is a decrease in the onset potential and a more evident increase in the maximum current when the tungsten oxide and nickel tungstate are added due to the auxiliary effect these species exert on Pt. Figure S5 shows

Preprints (www.preprints.org) | NOT PEER-REVIEWED | Posted: 27 November 2023 doi:10.20944/preprints202311.1641.v1

the corresponding chronoamperometric curves for the different materials with ethanol and glycerol. As in the case of voltamperograms, adding TO and NiT-TO to the catalyst formulation leads to higher currents and a lower current decay, corroborating the promoting effect of the tungsten oxide and the nickel tungstate.

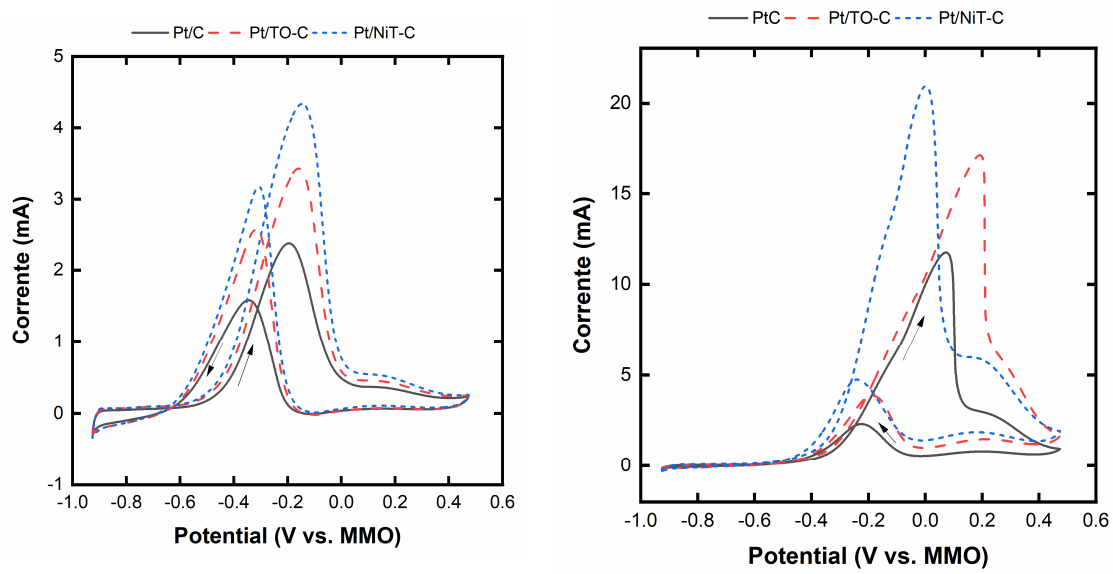

(**a**) (**b**)

Figure 6. (a) Ethanol, and (b) Glycerol electro-oxidation curves of the different electrocatalysts in 1 mol L^{-1} alcohol and 1 mol L^{-1} KOH.

Table 2. Onset potential and maximum current for each catalyst.

Catalyst	Onset potential for ethanol/glycerol (V vs. MMO)	Maximum current for ethanol/glycerol (mA)
Pt/C	–0.471/–0.327	2.3/11.7
Pt/TO-C	–0.500/–0.320	3.3/17.2
Pt/NiT-TO-C	–0.508/–0.301	4.4/20.8

3. Discussion

The results displayed in Figure 1 evidence that the increase in the PWA concentration reduces the amount of phosphorus and tungsten that remain in the NCC structure. One possible explanation lies in the observation of Zhao et al. [45], where the acid concentration affects the macrostructure of the resulting hydrolysis products. The authors observed that an increase in the acid concentration increased cellulose hydrolysis, exposing more nanofibers due to a more aggressive treatment. Nevertheless, the increase in the acid concentration also tends to agglomerate the larger fibers of the MCC, which may reduce the contact between the MCC and the PTA, decreasing the PW percentage of the hydrolyzed samples. On the other hand, the exposed MCC surface (although smaller) undergoes more severe hydrolysis, resulting in NCC of smaller sizes, as corroborated by the TEM images and the slight decrease in thermal stability. In the case of using ethanol as solvent, there are more noticeable changes in the MCC to NCC transition. In particular, the O content drastically increases compared to water as solvent. Ethanol might reduce the aggregation of the MCC fibers, as it may be able to better interact with the MCC fibers given its lower dipolar moment, exposing more surface to the PWA attack. PWA is known to be a strong oxidizing agent [46], increasing the O percentage. For this reason, we select the aqueous PWA hydrolysis with an acid concentration of 1 mol L^{-1}.

 doi:10.20944/preprints202311.1641.v1

Figure 2 evidences that the solvent and impregnation time strongly influence the subsequent impregnation process for preparing the binary oxide NiT. The most favorable condition for maximizing the Ni percentage balanced with W is achieved after using ethanol as the impregnation solvent and 1 h for this treatment. It then seems that ethanol promotes the interaction of the NCC template and the nickel precursor due to its smaller polarity, rendering a more Ni-charged material. On the other hand, an excessive impregnation time unbalances the Ni/W proportion, leading to a W-overcharged material.

The XRD patterns also confirm that more NiT is formed when ethanol is used as the solvent, as the NiT diffraction peaks emerge as the highest peak in the E1 and E6 samples, which is not the case in the W1 and W6 samples, where the peaks attributed to TO are higher than NiT ones. Moreover, the E1 NiT-TO sample presents the smallest average crystallite sizes, which is desirable for application in electrocatalysis as it exposes the highest surface area. For these reasons, the calcinated NiT-TO E1 material is selected for preparing the potential Pt electrocatalyst (Pt/NiT-TO-C) to be applied in the glycerol and ethanol electro-oxidation, in addition to Pt/TO-C. Finally, it is important to note that, despite the excess of nickel in the ethanol-based samples, diffraction peaks associated with NiO are not visible. Thus, NiO could be present in the form of an amorphous oxide. The formation of this multiphase material may be of interest based on the promotional properties of TO, NiT, and NiO by itself, which may be further promoted by a synergistic effect.

To provide electronic conductivity to the TO and NiT materials, they were mixed with carbon, and, in the sequence, Pt was deposited onto this hybrid support. The XRD patterns confirm the successful deposition of Pt in the form of small nanocrystals. These values are close to that of commercial 20 wt.% Pt/C (3.2 nm, Novocell, São Paulo, Brazil, https://www.novocell.ind.br/pt/produtos/componentes/material-catalitico). The achieved low particle sizes are typical of the formic acid reduction method used in this work [47]. Also, the formation of nanometric TO and NiT can help to form small Pt nanocrystals. Figure 5 displays the blank voltammograms of the prepared materials compared to the commercial Pt/C. The three materials present the same shape, with the typical peaks ascribed to the hydrogen adsorption/desorption region and the PtO formation and reduction. No apparent voltammetric signal can be assigned to TO and NiT, which is interesting from the point of view of the stability of these auxiliary species.

The ethanol and glycerol electro-oxidation curves reveal the promotional effect that TO and, especially NiT, exert on Pt. A decrease in the onset potential can be observed, primarily attributable to the bifunctional effect coming from the presence of TO in the Pt/TO-C material and the mixed oxide present in the Pt/NiT-C. More noticeable is the increase in the maximum current densities. The combined bifunctional effect, which assists in removing more efficiently the alcoholic carbonaceous residues that adsorb onto the Pt surface, and the possible electronic effect coming from the Pt/TO and Pt/NiT interactions, can be responsible for a more rapid refreshment of the Pt surface [48]. This favorable tendency is maintained in the chronoamperometric measurements, where the Pt/NiT-C outperforms Pt/TO-C > Pt/C, in addition to the slower current decay. Therefore, the addition of TO and, for the first time for the ethanol and glycerol electro-oxidation in alkaline medium, NiT in the nanometric form to the Pt on carbon formulation has demonstrated to possess a promotional effect on the Pt electrocatalyst, postulating the Pt/NiT-C for its application in Direct Ethanol and Direct Glycerol Alkaline Fuel Cells/Electroreformers.

4. Materials and Methods

Sulfuric acid (95-97 wt.%), ethanol (99.8 wt.%), microcrystalline cellulose (powder), phosphotungstic acid ($H_3PW_{12}O_{40}$ xH_2O, >99.9 wt.%), hexachloroplatinic acid (H_2PtCl_6 xH_2O, 38 wt.% Pt), nickel(II) nitrate hexahydrate (99 wt.%) were purchased from Sigma-Aldrich (Barueri, São Paulo, Brazil). Formic acid (85 wt.%), 2-propanol (99.5 wt.%), and KOH (85 wt.%) were acquired from Dinâmica (Indaiatuba, São Paulo, Brazil). Glass microfiber filter paper GF/F 125 mm was purchased from Hexis Científica (Jundai, São Paulo, Brazil).

 doi:10.20944/preprints202311.1641.v1

NCC was prepared by mixing in a test tube 0.15 g of MCC in 0.625 mL of ultrapure water (or ethanol) and the required amount of PWA to achieve the desired acid concentration. The reactional mixture was heated for 1 h at 80 °C. Next, the product was extracted from the tube, filtered, and washed thoroughly until neutralization of the supernatant.

The produced NCC from 1 mol L^{-1} PWA was subsequently impregnated with 10 mL of 0.2 mol L^{-1} $Ni(NO_3)_2$ ethanol or water solution, heated at 80 °C for 1 or 6 h. Afterward, the impregnated sample was calcinated at 600 °C in air atmosphere for 6 h to render the TO or NiT material.

The Pt/TO-C and Pt/NiT-C catalysts were prepared by the formic acid reduction method. In a typical procedure, 80 mg of the support, formed by combining 30 mg of TO or NiT and 50 mg of Vulcan XC-72 (Cabot Corp., Tokyo, Japan) carbon black, were dispersed in a 0.1 mol L^{-1} formic acid solution. The mixture was heated up to 80 °C, in which the necessary volume of the Pt precursor solution (50 g L^{-1} of $H_2PtCl_6{\cdot}6H_2O$) was dropwise added to the solution. After completing the addition of the Pt precursor, the temperature was maintained for an extra hour, leaving the solution to cool down and settle for 12 hours. The catalyst powder was then filtered (cellulose acetate membrane, 0.22 μm, 47 mm diameter) and thoroughly washed with boiling water. Finally, the catalysts were dried in an oven at 90 °C for one hour, checking the final mass.

The prepared materials were characterized by X-ray diffraction obtained in the D8 Focus Diffractometer (Bruker, Billerica, Massachusetts, USA) using the Cu K_α radiation (wavelength 0.15418 nm) applying a source voltage of 40 kV and a current of 30 mA. The applied 2θ angles varied from 10 to 90° at a rate of 1° min^{-1}, with a step of 0.05°. Scherrer's equation was applied to estimate the average crystal sizes (D), where λ is the wavelength of the X-ray source, $\beta_{1/2}$ is the width of the peak at half-height, and θ is the angle of the peak position.

$$D = \frac{0.9\lambda}{\beta_{1/2}\cos\theta} \quad (1)$$

Elemental analyses were performed according to the Brazilian Association of Technical Standards (ABNT, NBR E775, E777, E778 and E870). These analyses provided the mass percentages of the main elements in the different materials. Carbon (C), nitrogen (N), and hydrogen (H) were determined in a Perkin Elmer 2400 Series II CHN Elemental Analysis equipment (Waltham, Massachusetts, USA). The other components were determined using a Shimadzu X-ray Fluorescence (XRF) spectrometer (model EDX 720) with a rhodium tube as X-ray source (Kyoto, Japan). Oxygen (O) was calculated from the results obtained from CHN and XRF/EDX.

Thermogravimetry (TG) and derivative thermogravimetry (DTG) were obtained on a TA Instruments SDT Q600 (New Castle, DE, USA) from room temperature to 1000 °C (20 °C min^{-1}), using synthetic air (80 ± 0.5 of N_2 and 20 ± 0.5 of O_2 - purity > 99.999%) as the purge gas (flow rate of 60 mL min^{-1}). The analysis was performed on alumina crucibles, and the external standard employed for calibration was sapphire.

TEM images were obtained in a JEOL 1011 microscope at different magnifications in high vacuum. For sample preparation, a mass of 1 mg of samples was dispersed in 50 mL of ethanol, depositing 1 μL of the dispersion onto the copper mesh. The samples were dried for 24 h before executing the analysis.

Electrochemical characterization was carried out by cyclic voltammetry using a three-electrode glass cell in 1 mol L^{-1} KOH. The working electrode, a 5 mm reticulated vitreous carbon electrode, was prepared by dispersion 4 mg of catalysts in 1 mL of 2-propanol and 10 μL of a Nafion® emulsion (5 wt.% in a mixture of aliphatic alcohols, from IonPower (Tyrone, PA, USA)). A volume of 10 μL was deposited onto the working electrode and left to dry. The counter-electrode was a platinized Pt gauze, and a Hg/HgO/KOH (1 mol L^{-1}) was used as the reference electrode. The system was thoroughly purged with N_2 before the electrochemical measurements. The blank voltammograms were executed by cycling the potential between –0.926 and 0.424 V vs. MMO until obtaining a stable voltammetry in 1 mol L^{-1} KOH.

The alcohol electrochemical activity was carried out similarly to the blank voltammetries in 1 mol L^{-1} KOH and alcohol. In this case, the voltammetry limits were –0.8 V to 0.3 V vs. MMO, repeating

the cycles until obtaining similar profiles. Finally, the chronoamperometric curves, recorded after completing the cyclic voltammetries, were carried out for 30 minutes at –0.25 V vs. MMO. No normalization has been applied to the electrochemical measurement as all the prepared working electrodes possessed the same Pt mass loading.

5. Conclusions

NCC has demonstrated to be a suitable template for preparing nanosized TO and NiT. NCC can be readily prepared from the acid hydrolysis with PWA of MCC, with an optimum acid concentration of 1 mol L^{-1} to guarantee the formation of nanosized cellulose in aqueous medium. This NCC acts as an effective template to prepare NiT nanoparticles after preferential impregnation with ethanol for 1 h (to obtain the highest Ni deposition and the most equilibrated Ni/W ratio), rendering a mixed material with WO_3, $NiWO_4$, and, likely, NiO. These TO and NiT, when applied as co-catalysts to Pt, have evidenced a promotional effect on the ethanol and glycerol electro-oxidation in alkaline medium, enhancing the onset potential and, mainly, the current density. In this way, the oxide or binary oxides, prepared with the aid of NCC as template, can be postulated as effective auxiliary materials for platinum with potential application for alkaline Direct Ethanol and Direct Glycerol Alkaline Fuel Cells/Electroreformers to produce clean electricity or green hydrogen.

Supplementary Materials: The following supporting information can be downloaded at the website of this paper posted on Preprints.org. Table S1: Thermal parameters of the original MCC; Figure S1: a) Thermogravimetric profiles of the MCC and NCC, and (b) their corresponding weight derivate; Figure S2: Diffractograms of the MCC and NCC samples; Figure S3: TEM images of the MCC and NCC samples; Figure S4: TEM images of the resulting NiT materials after the thermal treatment of the NCC as a function of the solvent and impregnation treatment time; Figure S5: Chronoamperometry profiles of the different materials for in 1 mol L^{-1} alcohol and in 1 mol L^{-1} KOH (a) ethanol electro-oxidation (b) glycerol electro-oxidation at a potential of −0.25 V vs. MMO.

Author Contributions: Conceptualization, J.L.M., J.J.L. and G.F.G.; methodology, M.G.H, J.L.M., J.J.L. and G.F.G.; validation, J.L.M., J.J.L. and G.F.G.; formal analysis, J.J.L and G.F.G.; investigation, M.G.H; resources, G.F.G.; data curation, M.G.H, J.L.M., J.J.L. and G.F.G.; writing—original draft preparation, M.G.H, J.L.M., J.J.L. and G.F.G.; supervision, J.LM., J.J.L and G.F.G.; project administration, G.F.G.; funding acquisition, G.F.G.. All authors have read and agreed to the published version of the manuscript.

Funding: José J. Linares acknowledges Fundação de Apoio à Pesquisa do Distrito Federal (FAPDF, process n. 0193.001.473/2017). Grace F. Ghesti and Munique G.Guimarães acknowledges Coordenação de Aperfeiçoamento de Pessoal de Nível Superior (CAPES), Decanato de Pesquisa e Inovação da Universidade de Brasília (DPI/UnB) and FAPDF.

Data Availability Statement: The data presented in this study are available on request from the corresponding author. The data are not publicly available due to privacy.

Conflicts of Interest: The authors declare no conflict of interest.

References

1. Sertolli, A.; Gabnai, Z.; Lengyel, P.; Bai, A. Biomass Potential and Utilization in Worldwide Research Trends—A Bibliometric Analysis. *Sustainability* **2022**, *14*, 5515–5534, doi:10.3390/su14095515.
2. Gielen, D.; Boshell, F.; Saygin, D.; Bazilian, M.D.; Wagner, N.; Gorini, R. The Role of Renewable Energy in the Global Energy Transformation. *Energy Strateg. Rev.* **2019**, *24*, 38–50, doi:10.1016/j.esr.2019.01.006.
3. Singh, S.P.; Jawaid, M.; Chandrasekar, M.; Senthilkumar, K.; Yadav, B.; Saba, N.; Siengchin, S. Sugarcane Wastes into Commercial Products: Processing Methods, Production Optimization and Challenges. *J. Clean. Prod.* **2021**, *328*, 129453, doi:10.1016/j.jclepro.2021.129453.
4. Ungureanu, N.; Vlăduț, V.; Biriș, S.-Ștefan Sustainable Valorization of Waste and By-Products from Sugarcane Processing. *Sustainability* **2022**, *14*, 11089, doi:10.3390/su141711089.
5. Kabeyi, M.J.B.; Olanrewaju, O.A. Bagasse Electricity Potential of Conventional Sugarcane Factories. *J. Energy* **2023**, *2023*, 1–25, doi:10.1155/2023/5749122.

6. Macrelli, S.; Mogensen, J.; Zacchi, G. Techno-Economic Evaluation of 2nd Generation Bioethanol Production from Sugar Cane Bagasse and Leaves Integrated with the Sugar-Based Ethanol Process. *Biotechnol. Biofuels* **2012**, *5*, 22, doi:10.1186/1754-6834-5-22.
7. Dias, M.O.S.; Junqueira, T.L.; Cavalett, O.; Cunha, M.P.; Jesus, C.D.F.; Rossell, C.E.V.; Maciel Filho, R.; Bonomi, A. Integrated versus Stand-Alone Second Generation Ethanol Production from Sugarcane Bagasse and Trash. *Bioresour. Technol.* **2012**, *103*, 152–161, doi:10.1016/j.biortech.2011.09.120.
8. Mandal, A.; Chakrabarty, D. Isolation of Nanocellulose from Waste Sugarcane Bagasse (SCB) and Its Characterization. *Carbohydr. Polym.* **2011**, *86*, 1291–1299, doi:10.1016/j.carbpol.2011.06.030.
9. Lu, Q.; Cai, Z.; Lin, F.; Tang, L.; Wang, S.; Huang, B. Extraction of Cellulose Nanocrystals with a High Yield of 88% by Simultaneous Mechanochemical Activation and Phosphotungstic Acid Hydrolysis. *ACS Sustain. Chem. Eng.* **2016**, *4*, 2165–2172, doi:10.1021/acssuschemeng.5b01620.
10. Trache, D.; Tarchoun, A.F.; Derradji, M.; Hamidon, T.S.; Masruchin, N.; Brosse, N.; Hussin, M.H. Nanocellulose: From Fundamentals to Advanced Applications. *Front. Chem.* **2020**, *8*, 1–33, doi:10.3389/fchem.2020.00392.
11. Thomas, B.; Raj, M.C.; B, A.K.; H, R.M.; Joy, J.; Moores, A.; Drisko, G.L.; Sanchez, C. Nanocellulose, a Versatile Green Platform: From Biosources to Materials and Their Applications. *Chem. Rev.* **2018**, *118*, 11575–11625, doi:10.1021/acs.chemrev.7b00627.
12. Anžlovar, A.; Žagar, E. Cellulose Structures as a Support or Template for Inorganic Nanostructures and Their Assemblies. *Nanomaterials* **2022**, *12*, 1837–1907, doi:10.3390/nano12111837.
13. Laurent, S.; Boutry, S.; Muller, R.N. Metal Oxide Particles and Their Prospects for Applications. In *Iron Oxide Nanoparticles for Biomedical Applications*; Mahmoudi, M., Laurent, S., Eds.; Elsevier: Amsterdam, Netherlands, 2018; pp. 3–42 ISBN 978-0-08-101925-2.
14. Danish, M.S.S.; Bhattacharya, A.; Stepanova, D.; Mikhaylov, A.; Grilli, M.L.; Khosravy, M.; Senjyu, T. A Systematic Review of Metal Oxide Applications for Energy and Environmental Sustainability. *Metals (Basel).* **2020**, *10*, 1604–1623, doi:10.3390/met10121604.
15. Megía, P.J.; Vizcaíno, A.J.; Calles, J.A.; Carrero, A. Hydrogen Production Technologies: From Fossil Fuels toward Renewable Sources. A Mini Review. *Energy & Fuels* **2021**, *35*, 16403–16415, doi:10.1021/acs.energyfuels.1c02501.
16. Abohamzeh, E.; Salehi, F.; Sheikholeslami, M.; Abbassi, R.; Khan, F. Review of Hydrogen Safety during Storage, Transmission, and Applications Processes. *J. Loss Prev. Process Ind.* **2021**, *72*, 104569, doi:10.1016/j.jlp.2021.104569.
17. Bristowe, G.; Smallbone, A. The Key Techno-Economic and Manufacturing Drivers for Reducing the Cost of Power-to-Gas and a Hydrogen-Enabled Energy System. *Hydrogen* **2021**, *2*, 273–300, doi:10.3390/hydrogen2030015.
18. Siwal, S.S.; Thakur, S.; Zhang, Q.B.; Thakur, V.K. Electrocatalysts for Electrooxidation of Direct Alcohol Fuel Cell: Chemistry and Applications. *Mater. Today Chem.* **2019**, *14*, 100182, doi:10.1016/j.mtchem.2019.06.004.
19. Miller, H.A.; Lavacchi, A.; Vizza, F. Storage of Renewable Energy in Fuels and Chemicals through Electrochemical Reforming of Bioalcohols. *Curr. Opin. Electrochem.* **2020**, *21*, 140–145, doi:10.1016/j.coelec.2020.02.001.
20. Martins, C.A.; Fernández, P.S.; Troiani, H.E.; Martins, M.E.; Camara, G.A. Ethanol vs. Glycerol: Understanding the Lack of Correlation between the Oxidation Currents and the Production of CO2 on Pt Nanoparticles. *J. Electroanal. Chem.* **2014**, *717–718*, 231–236, doi:10.1016/j.jelechem.2014.01.027.
21. Souza, F.M.; Pinheiro, V.S.; Gentil, T.C.; Lucchetti, L.E.B.; Silva, J.C.M.; L.M.G. Santos, M.; De Oliveira, I.; Dourado, W.M.C.; Amaral-Labat, G.; Okamoto, S.; et al. Alkaline Direct Liquid Fuel Cells: Advances, Challenges and Perspectives. *J. Electroanal. Chem.* **2022**, *922*, 116712, doi:10.1016/j.jelechem.2022.116712.
22. Wala, M.; Simka, W. Effect of Anode Material on Electrochemical Oxidation of Low Molecular Weight Alcohols—A Review. *Molecules* **2021**, *26*, 2144, doi:10.3390/molecules26082144.
23. Zhao, G.; Fang, C.; Hu, J.; Zhang, D. Platinum-Based Electrocatalysts for Direct Alcohol Fuel Cells: Enhanced Performances toward Alcohol Oxidation Reactions. *Chempluschem* **2021**, *86*, 574–586, doi:10.1002/cplu.202000811.
24. Vyas, A.N.; Saratale, G.D.; Sartale, S.D. Recent Developments in Nickel Based Electrocatalysts for Ethanol Electrooxidation. *Int. J. Hydrogen Energy* **2020**, *45*, 5928–5947, doi:10.1016/j.ijhydene.2019.08.218.

25. Wala, M.; Simka, W. Effect of Anode Material on Electrochemical Oxidation of Low Molecular Weight Alcohols—A Review. *Molecules* **2021**, *26*, 2144, doi:10.3390/molecules26082144.
26. Vyas, A.N.; Saratale, G.D.; Sartale, S.D. Recent Developments in Nickel Based Electrocatalysts for Ethanol Electrooxidation. *Int. J. Hydrogen Energy* **2020**, *45*, 5928–5947, doi:10.1016/j.ijhydene.2019.08.218.
27. TSURUMURA, T.; YOSHIMOTO, N.; EGASHIRA, M.; MORITA, M. Electrocatalytic Activity of Platinum Nano-Particle Deposited on Tungsten Oxide for Anodic Oxidation of Ethanol. *Electrochemistry* **2012**, *80*, 916–918, doi:10.5796/electrochemistry.80.916.
28. Miecznikowski, K. WO3 Decorated Carbon Nanotube Supported PtSn Nanoparticles with Enhanced Activity towards Electrochemical Oxidation of Ethylene Glycol in Direct Alcohol Fuel Cells. *Arab. J. Chem.* **2020**, *13*, 1020–1031, doi:10.1016/j.arabjc.2017.09.005.
29. Zhang, D.-Y.; Ma, Z.-F.; Wang, G.; Konstantinov, K.; Yuan, X.; Liu, H.-K. Electro-Oxidation of Ethanol on Pt-WO[Sub 3]/C Electrocatalyst. *Electrochem. Solid-State Lett.* **2006**, *9*, A423–A426, doi:10.1149/1.2211807.
30. Tseung, A.C.C.; Chen, K.Y. Hydrogen Spill-over Effect on Pt/WO3 Anode Catalysts. *Catal. Today* **1997**, *38*, 439–443, doi:10.1016/S0920-5861(97)00053-9.
31. Tseung, A.C.C.; Shen, P.K.; Chen, K.Y. Precious Metal/Hydrogen Bronze Anode Catalysts for the Oxidation of Small Organic Molecules and Impure Hydrogen. *J. Power Sources* **1996**, *61*, 223–225, doi:10.1016/S0378-7753(96)02352-X.
32. Kumar, R.; Bhuvana, T.; Sharma, A. Nickel Tungstate–Graphene Nanocomposite for Simultaneous Electrochemical Detection of Heavy Metal Ions with Application to Complex Aqueous Media. *RSC Adv.* **2017**, *7*, 42146–42158, doi:10.1039/C7RA08047F.
33. Kumar, R.; Gupta, P.K.; Agrawal, A.; Nagarale, R.K.; Sharma, A. Hydrothermally Synthesized Reduced Graphene Oxide-NiWO 4 Nanocomposite for Lithium-Ion Battery Anode. *J. Electrochem. Soc.* **2017**, *164*, A785–A795, doi:10.1149/2.1181704jes.
34. Du, X.; Shao, Q.; Zhang, X. Metal Tungstate Dominated NiCo2O4@NiWO4 Nanorods Arrays as an Efficient Electrocatalyst for Water Splitting. *Int. J. Hydrogen Energy* **2019**, *44*, 2883–2888, doi:10.1016/j.ijhydene.2018.12.061.
35. Srirapu, V.K.V.P.; Kumar, A.; Srivastava, P.; Singh, R.N.; Sinha, A.S.K. Nanosized CoWO 4 and NiWO 4 as Efficient Oxygen-Evolving Electrocatalysts. *Electrochim. Acta* **2016**, *209*, 75–84, doi:10.1016/j.electacta.2016.05.042.
36. Hai, G.; Huang, J.; Cao, L.; Kajiyoshi, K.; Wang, L.; Feng, L. Hierarchical W18O49/NiWO4/NF Heterojunction with Tuned Composition and Charge Transfer for Efficient Water Splitting. *Appl. Surf. Sci.* **2021**, *562*, 150145, doi:10.1016/j.apsusc.2021.150145.
37. Somacescu, S.; Osiceanu, P.; Calderon Moreno, J.M.; Culita, D.C.; Neațu, F.; Trandafir, M.M.; Neațu, Ștefan; Kuncser, A.; Szijjártó, G.P.; Tálas, E.; et al. Design of Electrocatalysts with Reduced Pt Content Supported on Mesoporous NiWO4 and NiWO4-Graphene Nanoplatelets Composite for Oxygen Reduction and Hydrogen Oxidation in Acidic Medium. *Int. J. Hydrogen Energy* **2023**, *48*, 6317–6335, doi:10.1016/j.ijhydene.2022.04.270.
38. Shi, M.; Tong, X.; Li, W.; Fang, J.; Chen, L.; Ma, C. Enhanced Electrocatalytic Oxygen Reduction on NiWO x Solid Solution with Induced Oxygen Defects. *ACS Appl. Mater. Interfaces* **2017**, *9*, 34990–35000, doi:10.1021/acsami.7b10891.
39. Adzic, R.R.; Marinkovic, N.S. Electrocatalyst for Alcohol Oxidation in Fuel Cells 2001, 1–7.
40. Kumaresan, A.; Arun, A.; Kalpana, V.; Vinupritha, P.; Sundaravadivel, E. Polymer-Supported NiWO4 Nanocomposites for Visible Light Degradation of Toxic Dyes. *J. Mater. Sci. Mater. Electron.* **2022**, *33*, 9660–9668, doi:10.1007/s10854-021-07643-2.
41. Rosal, F.J.O.; Gouveia, A.F.; Sczancoski, J.C.; Lemos, P.S.; Longo, E.; Zhang, B.; Cavalcante, L.S. Electronic Structure, Growth Mechanism, and Sonophotocatalytic Properties of Sphere-like Self-Assembled NiWO4 Nanocrystals. *Inorg. Chem. Commun.* **2018**, *98*, 34–40, doi:10.1016/j.inoche.2018.10.001.
42. Afify, H.H.; Hassan, S.A.; Obaida, M.; Moussa, I.; Abouelsayed, A. Preparation, Characterization, and Optical Spectroscopic Studies of Nanocrystalline Tungsten Oxide WO3. *Opt. Laser Technol.* **2019**, *111*, 604–611, doi:10.1016/j.optlastec.2018.10.036.
43. B, S.; Divyashree, P.; Dhanekar, S.; Dwivedi, P. Sensing Demonstration and Scalable Production of Nanostructured WO3 FET. *Opt. Mater. (Amst).* **2022**, *134*, 113027, doi:10.1016/j.optmat.2022.113027.
44. Monshi, A.; Foroughi, M.R.; Monshi, M.R. Modified Scherrer Equation to Estimate More Accurately Nano-Crystallite Size Using XRD. *World J. Nano Sci. Eng.* **2012**, *02*, 154–160, doi:10.4236/wjnse.2012.23020.

45. Zhao, H.; Kwak, J.; Conrad Zhang, Z.; Brown, H.; Arey, B.; Holladay, J. Studying Cellulose Fiber Structure by SEM, XRD, NMR and Acid Hydrolysis. *Carbohydr. Polym.* **2007**, *68*, 235–241, doi:10.1016/j.carbpol.2006.12.013.
46. Noshi, M.N. Phosphotungstic Acid Hydrate. In *Encyclopedia of Reagents for Organic Synthesis*; John Wiley & Sons, Ltd.: Chichester, UK, 2013; pp. 1–8.
47. Pinheiro, A.L.N.; Oliveira-Neto, A.; De Souza, E.C.; Perez, J.; Paganin, V.A.; Ticianelli, E.A.; Gonzalez, E.R. Electrocatalysis on Noble Metal and Noble Metal Alloys Dispersed on High Surface Area Carbon. *J. New Mater. Electrochem. Syst.* **2003**, *6*, 1–8.
48. Fu, X.; Wan, C.; Huang, Y.; Duan, X. Noble Metal Based Electrocatalysts for Alcohol Oxidation Reactions in Alkaline Media. *Adv. Funct. Mater.* **2022**, *32*, doi:10.1002/adfm.202106401.